

1 **Flexural Modeling of the Colville Foreland Basin, Northern Alaska**

2 **M.H. Quddusi¹, and M. Pirouz¹**

3 ¹Department of Geosciences, The University of Texas at Dallas, Richardson, Texas, USA

4 Corresponding author: Muhammad Quddusi (hassan.quddusi@utdallas.edu)

5 **Key Points:**

- 6
- The elastic thickness of the Arctic Alaska microplate is 13-16 km
 - No influence of subsurface dynamic loads on the bending plate
 - A simple 3D flexure model predicts accurate deflection of the Colville foreland basin
- 7
- 8
- 9

10 Abstract

11 In this study, we model the flexure of the Colville foreland basin in northern Alaska and calculate
12 the effective elastic thickness (T_e) of the Arctic Alaska terrane with a simple 3D flexural model.
13 Previous studies show that the elastic thickness of northern Alaska is 65 km; however, the
14 wavelength of the Colville foredeep is considerably shorter for such an elastic thickness and
15 indicates a thinner elastic thickness for the area. Seismicity of crust, as a direct indicator of the
16 mechanical strength, reduces considerably at a depth of 25 km in northern Alaska. We address
17 these contrasting observations with a 3D flexural model to better understand elastic thickness
18 constraints for the north of the Alaska lithosphere. We constrained Colville basin geometry with a
19 structural map of the foredeep, where the maximum depth reaches 8 km towards the southwest of
20 the basin. The flexural deflection model of northern Alaska considers various parameters, and
21 results are compared to the observed data to obtain the best fit model. We applied basin and
22 topographic loads, including a crustal root load with a ratio of 3.4-4.5 times to modern topography.
23 Our obtained elastic thickness value is 13-16 km, with less than a 3% average misfit between the
24 model and the observation. The results of this study indicate that the Colville basin geometry is
25 mainly controlled by loads of the Brooks Range and basin deposits, and additional loads or density
26 anomalies in the crust are not required for the deflection of the basin.

27

28

29 Plain Language Summary

30 The Earth's outermost solid layer is called the lithosphere, which bends in response to the weight
31 of the mountain on the Earth's surface and the gravitational pull of high-density mantle in the
32 subsurface. The elastic strength of the plate defines the shape of the deflection. We calculate the

33 wavelength of this bending and thickness of the lithosphere, which behaves as an elastic plate, and
34 compared it with the observation. In this study, we used a 3D modeling code to calculate the elastic
35 thickness of the lithosphere in northern Alaska, where the Arctic Alaska plate bends downward in
36 response to the weight of the Brooks Range mountains and the Colville foreland basin. The results
37 of this study indicate that the elastic thickness of the lithosphere in northern Alaska is 13-16 km.
38 The low value of elastic thickness suggests that the north Alaska lithosphere has thin elastic
39 strength.

40

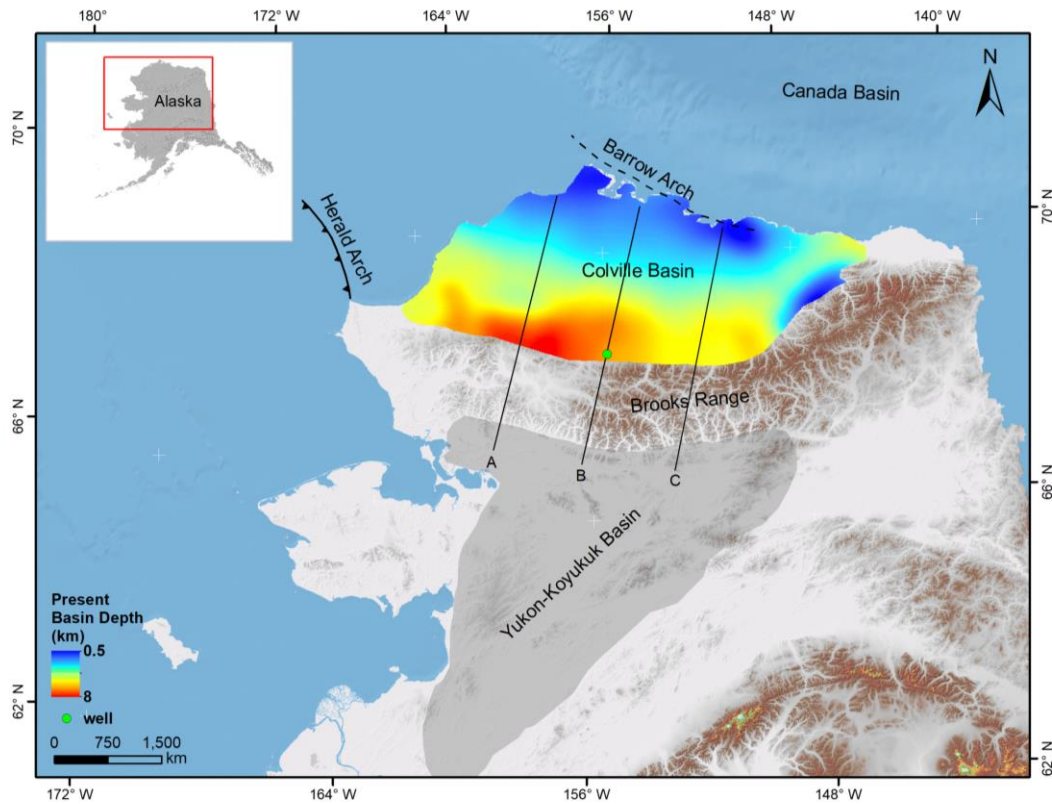
41 **1. Introduction**

42 Foreland basins in collisional zones are associated with down warping of the lithosphere as a result
43 of the loading of mountain front and accumulating sediments in the basin (Beaumont, 1981;
44 DeCelles, 2012; Karner & Watts, 1983), and their architecture offer essential insights into the
45 mechanical strength of the lithosphere. Subsurface loads may also contribute to loading, either by
46 static (e.g., density variations of the subducting slab and the associated lithospheric root) or
47 dynamic forces supported by mantle flow (Garcia-Castellanos, 2002; Pirouz et al., 2017). In this
48 study, we focus on the Colville foreland basin underlying the east-west trending North Slope of
49 Alaska (Figure 1). This basin is formed in response to the Brooks Range orogeny due to collision
50 and clastic volume shed between the Arctic Alaska microplate and an oceanic island-arc in the
51 Jurassic and Early Cretaceous (Box, 1985; Bird & Molenaar, 1992; Houseknecht, 2019; Moore et
52 al., 1994).

53 Geometry and sedimentary record of the Colville basin play a significant role in exploring the
54 dynamics of the northern Alaska and geomechanics of the lithosphere. Comparing the Colville

55 basin's wavelength with modern systems like Zagros and Taiwan enables us to have the first order
 56 of lithospheric elastic thickness estimation. The Zagros foreland basin width is approximately 450
 57 km and elastic thickness about 50 km (Pirouz et al., 2017), and in the Taiwan foreland basin, the
 58 basin width is 110 km; and elastic thickness is 13 km (Lin & Watts, 2002). The elastic thickness
 59 for the Colville basin with 200 km width is identified as 65 km (Nunn et al., 1987); however, by
 60 comparison with other foreland basins, it seems reported elastic thickness for this basin is
 61 considerably overestimated concerning the basin wavelength.

62



63

64 Figure 1. Modern plate setting of northern Alaska. Brooks Range fold and thrust belt are flanked on the north and
 65 south by Colville and Yukon-Koyukuk foreland basins. The observed Colville foreland basin depth is adopted from
 66 (Bird & Houseknecht, 2011).

67 A recent study involves 3D forward modeling of crustal density variations and Bouguer anomalies
68 of whole Alaska carried out by Torne et al. (2020). Their results highlight thick crust about 45 km
69 beneath the Brooks Range, and beneath the Colville basin, it gradually decreases by a few
70 kilometers. Furthermore, seismic events that mostly take place in the brittle zone of the crust
71 (Maggi et al., 2000) can also be used to rough constrain the elastic strength of the lithosphere. In
72 the Arctic Alaska region, the frequency of earthquakes drops dramatically at a depth of 25 km; this
73 observation is difficult to reconcile with the proposed 65 km elastic thickness by Nunn et al.
74 (1987).

75 The first deflection study in the Alaska region was carried out by Nunn et al. (1987) by modeling
76 a simple 2-D flexure of the Colville foreland basin. Their results suggest that the topographic and
77 basin loads are insufficient to produce the observed deflection, and gravity signals are
78 characterized by a local gravity minima representing mass deficit beneath the belt and basin. They
79 inferred that an additional subsurface load is required to make present-day basin geometry. In this
80 study, we estimate the effective elastic thickness (T_e) of the northern Alaska lithosphere and
81 address how the geometry of the Colville foreland basin relates to the orogenic loads posed by the
82 Brooks Range fold and thrust belt. We constrain the 3D geometry of the Colville foreland basin
83 with a published structural map of the foreland depth (Bird & Houseknecht, 2011). We model the
84 flexure of northern Alaska using a simple 3D elastic plate flexural bending model. Besides, we
85 also evaluate the possibility of additional subsurface loads. To validate the computed elastic
86 thickness from the flexural model, we calculate free-air gravity anomalies from the obtained
87 flexural model and compare it to the observed gravity data. We show that a flexural model based
88 on the weight of the Brooks Range and the Colville foreland basin fits well with the observed
89 present-day geometry of the foreland and the gravity data. Recent studies show that 3D flexural

90 solutions constrain better results for basin geometry, spatial/temporal variations in crustal
91 parameters, and elastic thickness compared with 2D models by applying a more realistic load of
92 topography and basin deposits (Curry et al., 2019; Pirouz et al., 2017). A recent reconstruction of
93 the Arabian plate deflection using a 3D approach shows that the topographic and basin loads and
94 the weight of crustal root models an accurate foreland basin geometry (Pirouz et al., 2017).
95 Geological observations in forward flexural modeling reconstruct better estimates for lithospheric
96 elastic thickness to compare with gravity data. In contrast, observed gravity offers better insights
97 for calculating the load posed by the crustal root (Pirouz et al., 2017).

98

99 **2. Geological and Geophysical Framework**

100 **2.1. Tectonic Evolution**

101 Alaska is a landmass formed by an amalgamation of several litho-tectonic terranes of varying
102 origins that were thoroughly assembled by the Late Cretaceous (Fuis et al., 2008; Moore & Box,
103 2016; Plafker & Berg, 1994). During the Jurassic and Early-Cretaceous, two major tectonic events
104 dominated northern Alaska. In the Early-Cretaceous, the Arctic Alaska microplate collided with
105 an oceanic arc-continent complex and bent downward in response to the collision. Simultaneously,
106 on the opposite side of the plate, towards the east, rifting occurred that led to the opening of the
107 present-day Canada basin (Mayfield et al., 1983; Sweeney, 1985). By the Mid-Cretaceous, the
108 collision resulted in the Brooks Range fold and thrust mountain belt and the associated foredeeps
109 on both sides of the range (Figure 1). The evolution of Arctic Alaska was accompanied
110 subsequently by counterclockwise rotation due to the opening of the Canada Basin. Although the
111 counterclockwise rotation model of Arctic Alaska and nearby terranes have been a topic of debate,

112 nonetheless, it is the most widely accepted and plausible explanation of the present-day tectonic
113 setting. For example, using geological and geophysical data Embry (1990) also supported the
114 hypothesis of the counterclockwise rotation model. An extensive discussion of all the terrane
115 nomenclature of Alaska is beyond the scope of this study; the reference is made to (Fuis et al.,
116 1997; Fuis et al., 2008; Moore et al., 1994; Moore & Box, 2016; Plafker & Berg, 1994) where a
117 compilation of most of the existing literature on the subject can be found.

118 The Present-day North Slope of Alaska consists of the Arctic Alaska terrane that constitutes the
119 Brooks Range fold and thrust belt and the Colville foreland basin (Figure 1) north of the Brooks
120 Range (Bird, 2001; Moore et al., 1994; Miller, 1994; Plafker & Berg, 1994). Towards the south
121 of the Brooks Range lies a Cretaceous age foreland basin called the Yukon-Koyukuk basin that
122 extends into the western Alaska region (Patton & Box, 1989). This range is about 1000 km long
123 and 300 km wide arcuate belt consisting of a series of imbricate thrust sheets with obduction of
124 ophiolites emplaced onto the southward (present coordinates) subducting continental Arctic
125 Alaska terrane. The estimated 580 km of crustal shortening occurred in some parts of the Brooks
126 Range (Mull, 1982; Nunn et al., 1987; Patton et al., 1994). The northern boundary of the Colville
127 basin is an Atlantic-type rifted continental margin (Grantz et al., 1994; Grantz & May, 1982) that
128 extends into the shoreline of Alaska where a broad subsurface basement ridge, the Barrow Arch,
129 developed during the rifting episode from Jurassic to Early Cretaceous. The basin extends offshore
130 toward west under the Chukchi Sea into the northwestward-trending Herald Arch and the
131 northward-trending Chukchi platform. These geological features are remnants of a late Paleozoic
132 to Early Mesozoic south-facing Arctic continental margin. On the far east, the basin narrows down
133 along the Alaska-Canada border (Bird, 2001).

134 **2.2. Tectonostratigraphic Sequences**

135 The North Slope of Alaska is underlain with rocks as early as the Late Proterozoic. Stratigraphic
136 records of the North Slope of Alaska is subdivided into four primary sequences based on tectonic
137 history, genetic relations, and origin (Bird, 2001; Hubbard et al., 1987). The oldest sequence, the
138 Franklinian sequence, holds a clue to complex geologic history due to deformation caused by
139 Ellesmerian orogeny. This sequence mostly consists of a Pre-Devonian deformed and
140 metamorphosed basement complex (Bird & Houseknecht, 2011; Grantz & May, 1982). The
141 basement complex is shallower near the Barrow Arch and is most profound at the northern edge
142 of Brooks Range. A regional unconformity developed with the Ellesmerian orogeny and the
143 Ellesmerian sequence was deposited on the passive margin of the Arctic shelf. This sequence, from
144 Mississippian to Triassic age, consists of carbonate and clastic continental shelf deposits (Bird,
145 2001). Syn-rift deposits characterized by stacked sequences of southward prograding clinoforms
146 forms Beaufortian Sequence of Jurassic and Early Cretaceous. A prominent feature in this
147 sequence is the break-up unconformity, also known as the Lower Cretaceous Unconformity (LC
148 U), at the crest of the Beaufortian sequence. On a regional scale, this unconformity truncates the
149 reservoir and seal rocks near the Barrow Arch, playing a vital role in hydrocarbon entrapments.
150 More importantly, LCU defines the base of the oncoming clastic sediments of the Colville basin
151 (Figure 2), which is essential for constraining the geometry of the Colville basin for flexural
152 studies. Beaufortian is the last sequence which has the northerly source of sediments. The Brookian
153 sequence is derived from the south due to the collisional orogeny of the Brooks Range. It comprises
154 progradation cycles characterizing dramatic sea level rises and substantial shifts of paleo shoreline
155 (Bird, 2001; Decker, 2007). Thick clastic sediments above 7620m (25,000 ft) are deposited into
156 the Colville basin (Houseknecht et al., 2009).

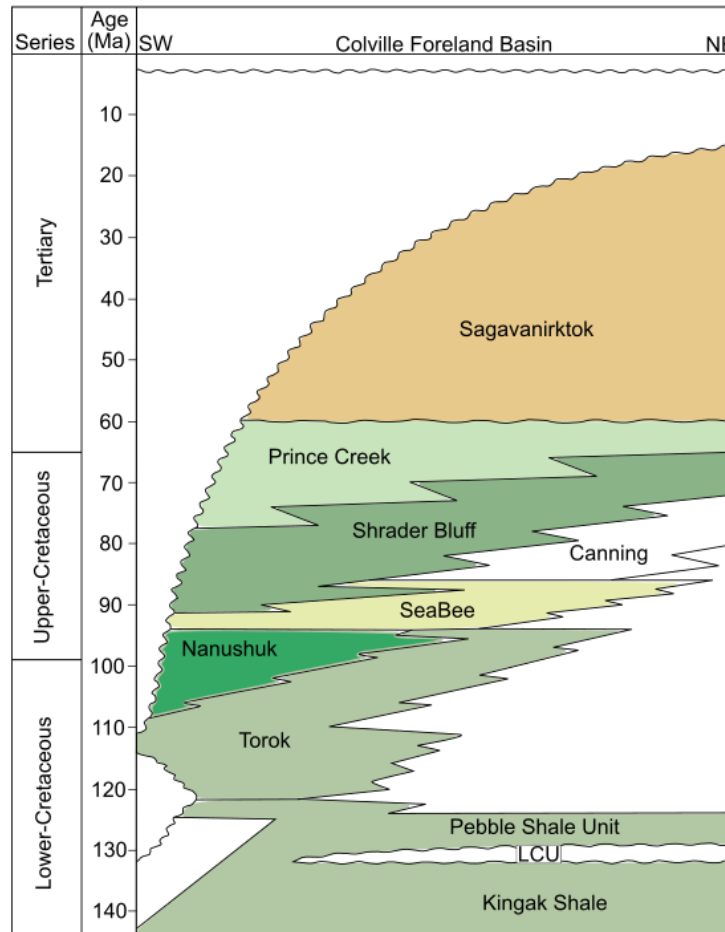
157

158 2.3. Geometry of Colville Foreland Basin

159 Colville basin is about 200 km wide with maximum depths of 8 km adjacent to the Brooks Range
160 toward its southern edge. A complete stratigraphic column of the Colville basin is shown in (Figure
161 2). The basin extends laterally from west to east spanning about 650 km area. The structural style
162 of the basin is a tapered wedge that shallows up-dip towards its northern edge close to Barrow
163 Arch, where the depth of the basin drops to 500 m. Investigation of seismic data shows massive
164 prograding clinoforms sequences in the Nanushuk and Torok formations, indicating a high rate of
165 sediment influx and large accommodation space in the Colville basin.

166 The seismic interpretation of the frontal Brooks Range and North Slope of Alaska shows evidence
167 of significant detachment surfaces that developed during the Tertiary deformation phase affecting
168 the southernmost part of the foredeep (Mull, 1982). The Kingak formation, which lies below LCU
169 (Figure 2), separates foreland sediments from the passive shelf margin acting as a surface for thrust
170 fault propagation and structural relief (Moore et al., 1994; Stier et al., 2014). Northward tectonic
171 transport of Early Brookian fold and thrust belt is evident in the southern part of the Colville basin,
172 which ceased possibly by Aptian (Moore & Box, 2016; Mull, 1982).

173



174

175 Figure 2. Stratigraphic column of the Colville basin. The Lower Cretaceous Unconformity LCU (ca. 133 Ma) is the regional unconformity
 176 separating Colville basin deposits from the passive margin. The Kingak shale constitutes the uppermost formation of the passive shelf margin.

177

178 2.4. Crustal Structure of Northern Alaska

179 Crustal architecture of continents is often studied using seismic tomographic imaging with active
 180 source experiments, e.g., S and P seismic receiver functions. In general, the Alaska continent
 181 shows substantial variability of crustal thickness due to variations in topography, multiple episodes
 182 of terrane accretion, and the influence of orogenic activity. Southern Alaska shows high variability
 183 of crustal thickness and more than 55 km crustal thickness observed near the Pacific margin,
 184 whereas central Alaska has an average of 32 km crustal thickness (Fuis et al., 2008). South and

185 south-central Alaska is extensively imaged by seismic broadband due to the active subduction of
186 the Pacific plate under Alaska (Miller et al., 2018). In contrast, the region north of the Brooks
187 Range has been sparsely imaged mainly due to quiescence in recent tectonic activity.

188 (TACT) was the first experimental imaging of the Brooks Range (Trans-Alaska-Crustal-Transect:
189 TACT) using seismic reflection and refraction methods covers an extensive profile from the south
190 to north (1350 km) covering entire Alaska (Fuis et al., 2008). In the northern Alaska segment of
191 TACT, the profile spanned from the coastal plains of Alaska through the Brooks Range. This study
192 identified an asymmetrical crustal root beneath the Brooks Range with 46 km thick crust. The
193 crustal evolution of northern Alaska is also defined by 3D modeling of Bouguer anomalies carried
194 out by Torne et al. (2020), highlighting regional lows ranging from -140 to -60 mGal in the
195 mountainous regions of the Brooks Range. This low regional trend extends north towards the
196 Colville foreland basin, where Bouguer anomalies range from -60 to -20 mGal. The overall trend
197 of regional low gravity anomalies highlights crustal thickening beneath the Brooks Range.
198 Towards the north of the Colville basin, the gravity anomalies abruptly change from low to high
199 values. The observed Bouguer anomalies near the shelf reach 180 mGal. This increase is attributed
200 to the thinner crust of the Beaufort shelf that is formed due to the rifting of the Canada Basin.

201

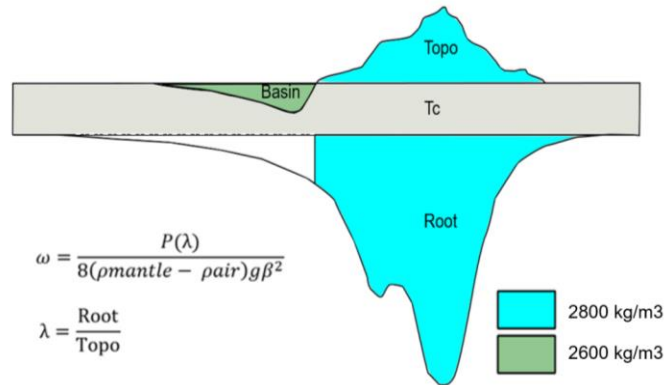
202 **3. Methods and Data**

203 **3.1. Flexure Model Description**

204 The lithospheric flexure studies have been mainly developed on two principle methods; the
205 forward modeling techniques (Cattin et al., 2001; Karner & Watts, 1983; Lyon-Caen & Molnar,
206 1983) and the inverse or spectral methods (Bechtel et al., 1990; Forsyth, 1985; Kaban et al., 2018;

207 Kirby & Swain, 2009; McKenzie & Fairhead, 1997). Recent advancements in computation have
208 also enabled various improvements in the spatial and spectral methods. For example, the finite-
209 element method (Arnaiz-Rodríguez et al., 2020; Simpson, 2017), the finite difference method
210 (Garcia-Castellanos et al., 1997; Tesauro et al., 2012), and the analytical solutions based on the
211 convolutional technique (Braitenberg et al., 2002; Wienecke et al., 2007). To calculate flexure
212 underneath the Arctic Alaska plate, we assume an elastic plate inviscid over a dense asthenosphere
213 in isostatic equilibrium (e.g., Turcotte & Schubert, 2002). The plate is flexed downward in
214 response to the topographic load, with contributions from the adjacent sediment-filled foreland
215 basin and the crustal root (Figure 3). An additional force also accompanies the downward flexure,
216 called the hydrostatic restoring pressure, caused by the replacement of mantle rocks by lighter
217 density crustal rocks. The crust beneath the load is effectively thickened by the amount by which
218 the Moho is depressed.

219 For deflection calculation, we use a new approach introduced by Pirouz et al. (2017). They applied
220 topographic load and basin load with density variation versus depth, and assume deflected
221 lithosphere filled with air (Pirouz et al., 2017, 2020), and a load of crustal root applied individually
222 with proportional ratio to topography (See figure 3; and see section 5.1 & 5.2 in Pirouz et al.,
223 2017). This method reconstructs a better deflection pattern that fits the observation since it has
224 been tested for several examples (Pirouz et al., 2020).



225

226 Figure 3. The conceptual model shows that the applied load is calculated from the excess thickness of the crust
 227 (topography and crustal root) and basin load colored in green. The equation calculates flexural parameters where T_c :
 228 the thickness of un-deformed crust, ω : max deflection, P : topographic load, ρ_{mantle} : density of mantle, ρ_{air} : density
 229 of air, g : gravity acceleration, β : flexural parameter and λ is the ratio between the thickness of crustal root and
 230 topographic height (adopted from Pirouz et al., 2017).

231

232 The modeling approach used in this study is based on an analytical solution derived from
 233 computing the partial derivatives of the 4th order of the equations that describe the bending of an
 234 elastic plate. This method has been tested previously in the convergent zones (Wienecke et al.,
 235 2007; Pirouz et al., 2017), and the results are also consistent and comparable with conventional
 236 spectral methods. The main advantage convolutional technique bears against the spectral approach
 237 is that the result is stable in irregular topography with a high spatial resolution (e.g., Wienecke et
 238 al., 2007). See supplementary material for details (Text S1).

239

240 3.2. Flexure Data, Gravimetric Analysis, and Workflow

241 The first step to model the flexure is to constrain the present-day geometry of the Colville foreland
 242 basin, whose base is highlighted by a regional unconformity known as the Lower Cretaceous

243 Unconformity (LCU). In this study, we use a published structural map of LCU adopted from (Bird
 244 & Houseknecht, 2011) to constrain the present-day basin geometry (Figure 4a). A complete surface
 245 load on the bending plate is characterized by both sediment infill and the adjacent range
 246 topography. To estimate the current topographic load, we use high resolution 60×60 m raster
 247 elevation grid; DEM (Digital Elevation Model) derived from (EDNA - Elevation Derivatives for
 248 National Applications) by US Geological Survey (2005); and for the basin load, we used the
 249 foreland depth map to obtain sediment thickness and took into account the density variation of the
 250 basin load with depth to calculated applied force from the basin. The deflection at each point is
 251 calculated iteratively using the equations described in supplementary material, and the elastic
 252 parameters used in the calculations are summarized in Table 1. The flexure model is tested by
 253 changing the elastic properties of the plate, and three cases of density variations are tried, and the
 254 output is summarized in Table 2 in section 4.2.

255 A range of models has been calculated by stepwise increasing the elastic thickness values between
 256 1 to 50 km. Similarly, the tested λ (root/topo ratio) ranges from 1 to 10, with a stepwise increase
 257 of 0.1. The iterative modeling approach is adopted to find the best fit between the observed and
 258 the predicted foreland depths by testing all possible solutions. The corresponding elastic thickness
 259 value at which the root-mean-square (RMSE) was minimum is the best fitting model. The
 260 deflection model is the predicted foreland surface derived from the flexure calculations.

261

262 Table 1. Summary of elastic paraments used in the calculation of the flexural model.

263

Constant	Symbol	Value	Units
Young's Modulus	E	1×10^{11}	Pa
Poisson's Ratio	σ	0.25	unitless quantity

Gravity Acceleration	g	9.81	m/sec^2
Mantle Density	ρ_{mantle}	3300	kg/m^3
Crustal Density	ρ_{crust}	2800	kg/m^3
Basin Density	ρ_{basin}	2600	kg/m^3
Air Density	ρ_{air}	1.200	kg/m^3

264

265

266

267

3.3. Gravimetric Analysis and Workflow

268 Gravimetric measurements at the Earth's surface are significant for studies of lithospheric flexure.

269 Gravity anomalies arising due to density variations in the lithosphere can be used to study the

270 isostatic balance of mountains on the Earth's surface. There are two methods typically used to

271 estimate the elastic thickness of the lithosphere with the gravity data (Watts, 2001). In forward

272 modeling technique, known load structures, e.g., a sedimentary basin or a seamount, are used in a

273 trial and error analysis to estimate the best fit elastic thickness of the lithosphere. In contrast, the

274 inverse spectral method uses the relationship between the observed gravity and topography. The

275 observed measures are subsequently inverted against the elastic plate predictions, giving estimates

276 of elastic thickness and other lithospheric parameters (Eshagh et al., 2020; Forsyth, 1985). The

277 estimates of elastic thickness from spectral methods are often over or under-estimated (McKenzie,

278 2010).

279 In this study, we also investigate the gravity signal of the Arctic Alaska microplate to validate our

280 flexural model results. However, we do not employ the conventional spectral methods to estimate

281 the effective elastic thickness; instead, free-air anomalies (FAA) are calculated from the flexure

282 model itself and then compared to the observed anomalies. We utilize the FAA dataset available

283 from World Gravity Map - WGM2012 (Bonvalot et al., 2012). WGM constitutes a set of gravity

284 anomaly maps and digital grids computed globally from available reference Earth's gravity and
285 the elevation models. The surface free-air anomaly dataset is derived from the EGM2008
286 Geopotential model and the ETOPO1 Global Relief Model. This dataset is a comprehensive free-
287 air anomaly that considers most surface masses, including atmosphere, land, ocean, inland seas,
288 lakes, ice caps, and ice shelves, and computations are based on accurate geodetic and geophysical
289 definitions of gravity anomalies. The anomaly grid is computed with a $1' \times 1'$ resolution, and the
290 reference density used for the Bouguer and the isostatic anomaly is 2670 km/m^3 . Furthermore, we
291 constrain the FAA using the Moho discontinuity boundary from the seismological Moho data of
292 entire Alaska assembled by Torne et al. (2020) and compare to the observed FAA and calculated
293 FAA from the best fitting deflection model. Calculations of the FAA are explained in the
294 supplementary material (Text S2).

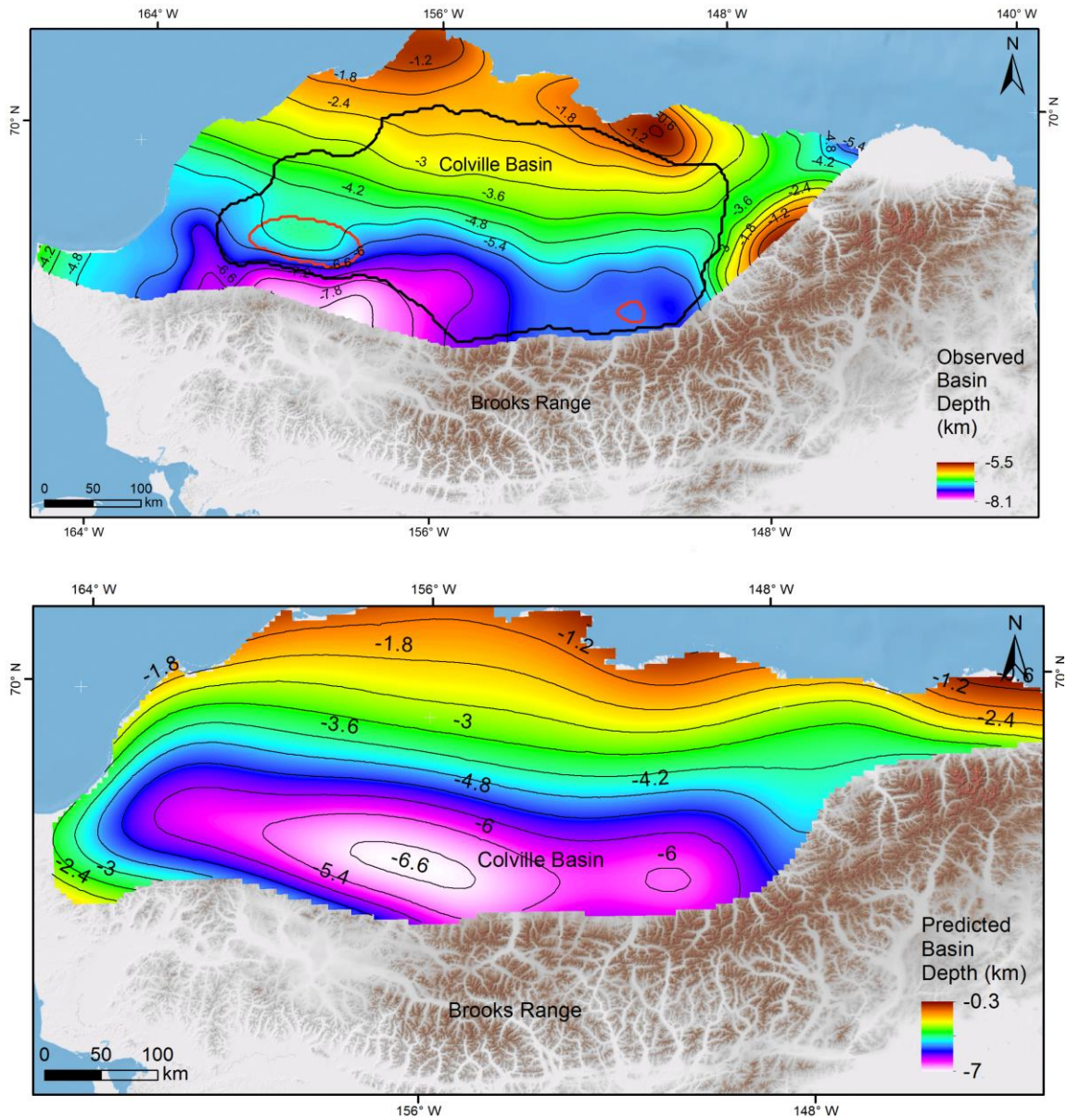
295

296 **4. Results and Discussion**

297 **4.1. Flexure Model of Colville Basin**

298 We present a simple 3D flexural model that reconstructs the Colville foreland basin geometry
299 (Figure 4). To avoid discrepancies in the output results, we systematically modified and clipped
300 regions of uplift and post-collisional deformation; for example, see two large antiforms (Figure
301 4a) that are ignored to compare the observed and the modeled foreland basin. A basement high,
302 Barrow Arch, significantly affects the northern part of the Colville basin. As a result, structural
303 relief of the foreland base abruptly changes between the high and low values. We exclude them to
304 avoid possibly overestimated or underestimated the importance of the elastic thickness. Our model
305 covers approximately $83,000 \text{ km}^2$ area of the basin exhibits an overall excellent correlation

306 between the observed and modeled foreland geometry with some systematic misfit. The observed
 307 misfit is shown along three cross-sections A, B, and C in Figure 5. For detailed cross sections in
 308 the Colville foredeep and misfit map, see supplementary material (Figure S3 and S6).
 309

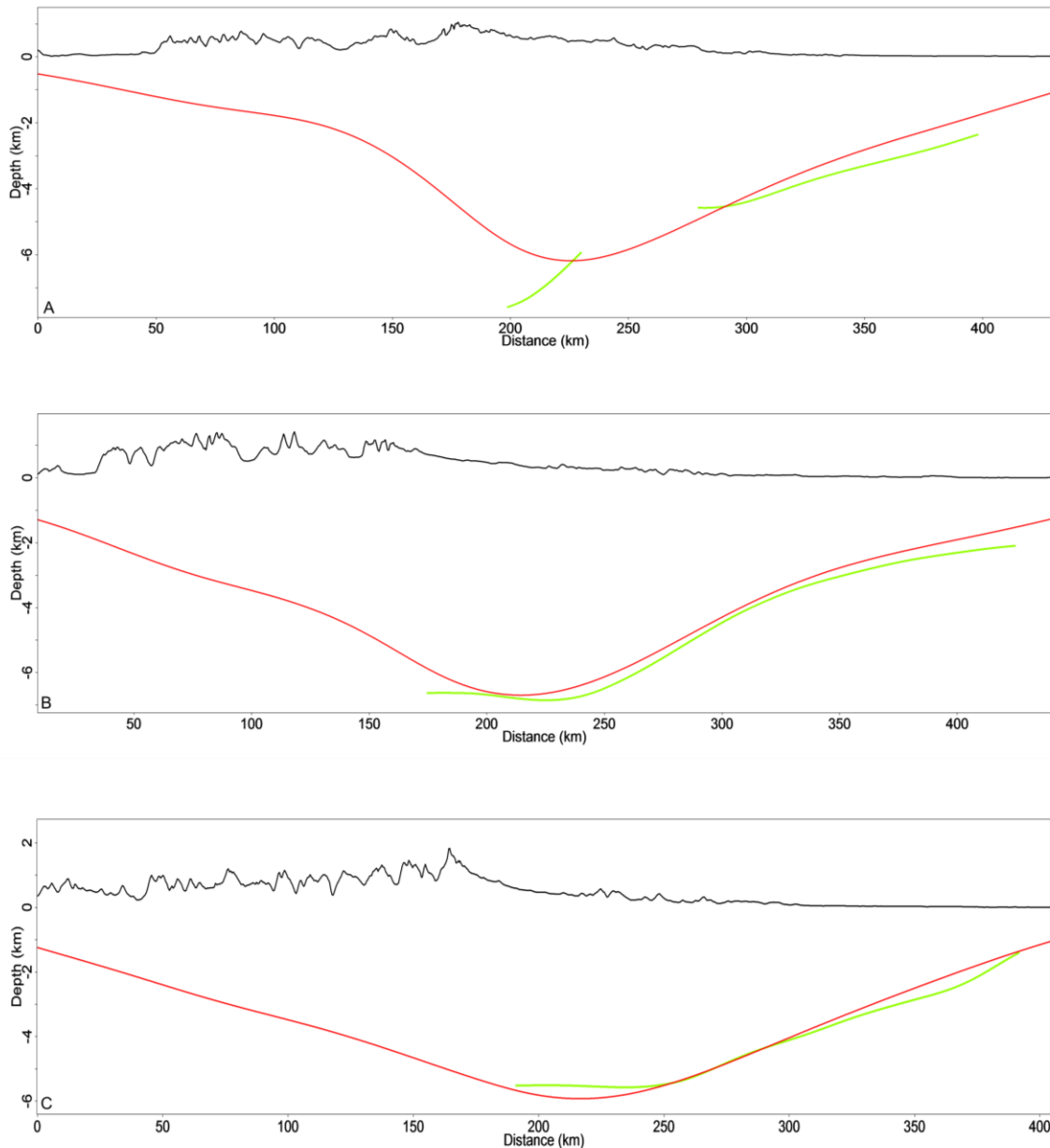


310
 311 Figure 4. Observed (a) and best model predicted depth (b) of the base of foreland sediments of the Colville basin. The area excluded for RMSE
 312 calculation is shown in panel (a). Black polygon in panel (a) corresponds to the RMSE area and red polygons show excluded areas from the RMSE
 313 calculation.
 314

315 Post-collisional deformation associated with the thrust front of the Brooks Range had minimal
316 effect on the basin geometry. In this section, we emphasize the causes of misfits between the
317 observed and modeled foreland depth and its important implications for the flexure model of the
318 Colville foreland basin. Following the collisional orogeny, the Brooks Range thrust system
319 experienced two significant phases of deformation. Early and Late Cretaceous tectonism is
320 characterized by crustal shortening and low relief duplex structures (Houseknecht & Wartes, 2013;
321 Moore et al., 2004; Wallace et al., 1997). The thrust belt also experienced a younger deformation
322 phase in Early Tertiary time (Stier et al., 2014). During the second phase, the fold and thrust sheets
323 were dominated by thick-skinned deformation. They consisted primarily of upright detachment
324 folds, whereas towards the north of the range front, the Early Cretaceous strata of the Colville
325 foreland basin experienced thin-skinned fold style deformation involving the formation of
326 anticlines. (See figure 15 in Moore & Box, 2016). Note that we exclude this deformed part from
327 RMSE calculation (figure 4a). The western part of the basin shows a weak correlation between the
328 observed and predicted foreland depth. This discrepancy arises mainly due to the second phase of
329 deformation, see Section A in figure 5a. Our model predicts shallower depths as compared to the
330 observed foreland depth. Section B shows the slightest misfit in the modeled foreland depth near
331 the northern part of the basin. We interpret this inconsistency as due to the uplifting effects of the
332 Barrow Arch basement high (Figure 5b). The model result yields the best correlation with the
333 observed data is shown in section C (Figure 5c), where the geometry of the foreland basin is
334 relatively uniform. See more correlating sections in the supplementary material (Figure S2).

335 We carefully considered all the misfits in the flexural model and conclude that these
336 inconsistencies are caused mainly by deformation processes and do not affect the robustness of the
337 model results. Our flexural model implies that the surface load posed by the Brooks Range

338 topography, a proportional subsurface crustal root associated with the orogen, and the overburden
 339 of the Colville basin sediments produce enough force to bend the Arctic Alaska microplate. We
 340 find that this model is very well correlated to the present-day foreland geometry of the Colville
 341 basin.



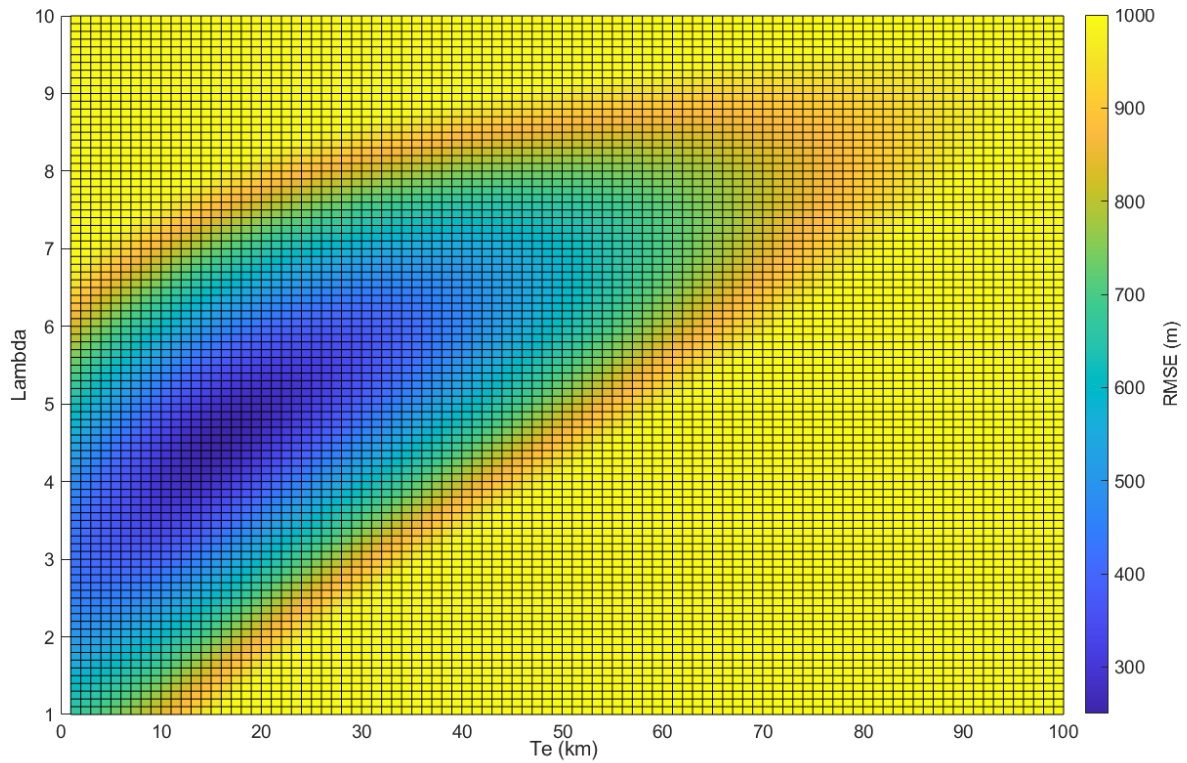
342
 343 Figure 5. Cross-sections (A, B, and C) in the study area showing observed and predicted flexure of the Colville basin. The green line represents the
 344 observed depth to the LCU, and the red line represents the modeled depth to the LCU. See figure 1 for the location of sections.

345

4.2. Estimating T_e value

346
347 The flexural model results provide a first-order calculation of the effective elastic thickness (T_e)
348 beneath the Colville foreland basin and offer insights into the long-term elastic strength of the
349 Arctic Alaska lithosphere. The optimum value of T_e is modeled by considering various elastic
350 parameters (Table 1). A significant varying elastic parameter is a function of density contrast
351 between the crust and mantle $\Delta\rho$. To obtain reliable density variation and unformed crustal
352 thickness, we obtained the FAA from the observed Moho depth (Torne et al., 2020) for a different
353 range of values for the mentioned variables. Our results show that $\Delta\rho = 300 \text{ kg/m}^3$ works best
354 where the minimum crust thickness is about 35 km (Miller et al., 2018). See supplementary
355 material figure S1. Our models indicate that the misfit error (RMSE) between the observed and
356 predicted foreland depth is lowest when ($\Delta\rho$) is minimum, and the corresponding T_e value is 13
357 km (Table 2). Solutions that still correlates precisely with the basin geometry (less than 3% error)
358 results from $\Delta\rho=300\text{-}500 \text{ kg/m}^3$, where the mantle density is about $3200\text{-}3300 \text{ kg/m}^3$, and the
359 average crustal density is 2800 kg/m^3 (Torne et al., 2020). We tuned the best fit models with
360 constant and varying elastic parameters (Table 1 and 2). Our models specify that the Arctic Alaska
361 microplate deflection can be realistically defined with a subsurface crustal root that is 3.4 - 4.5
362 times the modern topography of the Brooks Range mountain. Misfit error between the observed
363 and modeled foreland geometry is less than 3 %, and the best fit T_e value of 13-16 km (Figure 6).
364 FAA data is also used to model elastic thickness, but it does not precisely emphasize the elastic
365 thickness value like the geologic observation. In figure 7, we show the comparison between the
366 modeled FAA and the observed FAA. Note that changing 1.5 mGal in root mean square error value
367 will result in elastic thickness values between 40 and 100 km. However, it defines a better ratio
368 between topography and crustal root, which is about 4.5 for different elastic thickness values.

369



370

371 Figure 6. Root Mean Square Error (RMSE) between modeled and observed foreland depths as a function of an elastic thickness (T_e) and
 372 dimensionless scaling factor between root and topography (λ)

373

374

375 Table 2. Summary of modeling results using different density variation between mantle and crust. Obtained root to topography ratio, elastic
 376 thickness, RMSE of deflection models is listed below for five models.

377

Density Variation $\Delta\rho$ (kg/m^3)	Root/Topo Ratio (λ)	T_e (km)	Deflection RMSE (m)
700	5.8	21	327
600	5	16	285
500	4.5	16	252
400	3.9	14	225
300	3.4	13	205

378

379

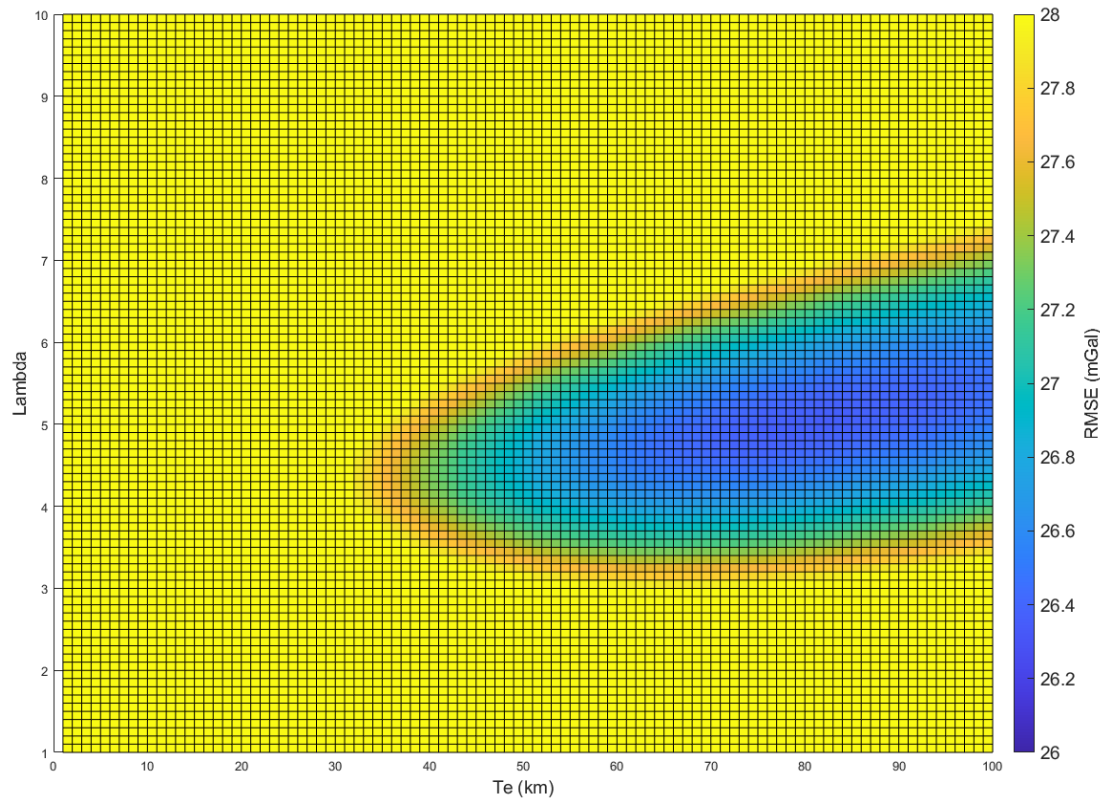


Figure 7. Root Mean Square Error (RMSE) between observed and modeled FAAs. Note the small change, 2mGal, in RMSE between observed FAA and models highlights a wide range of elastic thickness, e.g., $T_e=40$ to 100 km, and relatively better construction for crustal root-topography ratio.

Elastic thickness is a first-order proxy for the lithospheric strength, and low lithospheric strength results in a narrow and deep foreland basin (Burov & Diament, 1995; Watts & Burov, 2003). The Arctic Alaska lithosphere poses low resistance to the surface and subsurface-induced loads resulting in a deep short-wavelength basin. Our result shows that 13-16 km of elastic thickness for the Arctic Alaska lithosphere produces a basin that matches the observation. Our average misfit between model and observation is less than 252 meters in a basin with more than 6 km depth (about 3%).

The computed T_e value for northern Alaska is low compared to other foreland basins such as Appalachians and Zagros. However, it is within the range of many reported T_e values of foreland basins (Curry et al., 2019; Fosdick et al., 2014; Haddad & Watts, 1999; Lin & Watts, 2002). Simple

410 observation and comparison between the Colville basin's wavelength with active collisional zones
411 like Zagros also support the flexural model's results. The wavelength of the Zagros foreland basin
412 is approximately 450 km, and the reported elastic thickness is about 50 km (Pirouz et al., 2017).
413 In the Taiwan foreland basin, these values are 110 km and 10-13 km, respectively (e.g., Lin &
414 Watts, 2002). Considering these observations, computed 13-16 km T_e with 200 km wavelength of
415 the Colville basin fits this simple analysis well.

416 In general, old foreland basins have a large elastic thickness, but having a weak lithosphere in the
417 old basin is also possible. Foreland basins may inherit the low elastic thickness values as they
418 migrate over a passive margin and remain low for extended durations (Watts, 1992; Watts &
419 Burov, 2003; Angrand et al., 2018). In northern Alaska, we believe that during the collision of
420 Arctic Alaska terrane with the oceanic arc in Jurassic, the bending Arctic Alaska microplate
421 inherited the low elastic thickness and has considerably remained low after collisional tectonics
422 ended. Collision on the southern side of the plate (pre-rotation coordinates) started at the same
423 time as the arctic Alaska plate rifted away from the passive margin on its northern edge (Mayfield
424 et al., 1983; Sweeney, 1985), as shown by Desegaulx et al. (1991), we also believe it is likely that
425 the lithosphere and the foreland basin in northern Alaska acquired the size and width due to the
426 thermal state of ongoing rifting.

427 The rheological models affecting the long-term strength of an elastic lithosphere has long been a
428 topic of debate. The most widely accepted rheological models are; Crème Brulee (Jackson, 2002),
429 where the strength of the lithosphere mainly resides in the upper crust and mantle is considered
430 weak for accommodating long term stresses. On the other hand, the Jelly sandwich model (Afonso
431 & Ranalli, 2004; Burov, 2006) more realistically explains the multi-layer rheology of the Earth's
432 lithosphere. An important implication of these models is that the crust is either coupled or

433 decoupled from the upper mantle. The elastic thickness of a plate, as a result, is dependent on the
434 mechanical behavior of crust and mantle. A strong coupling between the crust and mantle suggest
435 high T_e values; on the other hand, low T_e values are associated with a mechanically decoupled
436 lithosphere (Brown & Phillips, 2000). We believe that strong driving forces in the mantle are
437 necessary for Alaska because the continent has a complex tectonic history of orogenesis and
438 accretion of far traveled terranes. In northern Alaska, this view agrees with the presence of a thick
439 lithosphere beneath the Brooks Range, as shown by Torne et al. (2020). Our results, therefore,
440 support strong upper mantle rheology, which in the case of northern Alaska, is decoupled from the
441 lower crust. However, our results do not support the idea of high elastic strength and a strong cold
442 lithosphere, as postulated by Torne et al. (2020). Contrarily, the flexural model results show
443 weakness in the elastic strength. Low T_e suggests that the mechanical weakness is possibly due to
444 the lithospheric extension associated with the rifting on the opposite side of the Arctic Alaska
445 microplate that initiated the collision forming the Brooks Range and the Colville basin.

446

447 **4.3. Implication for Subsurface Load**

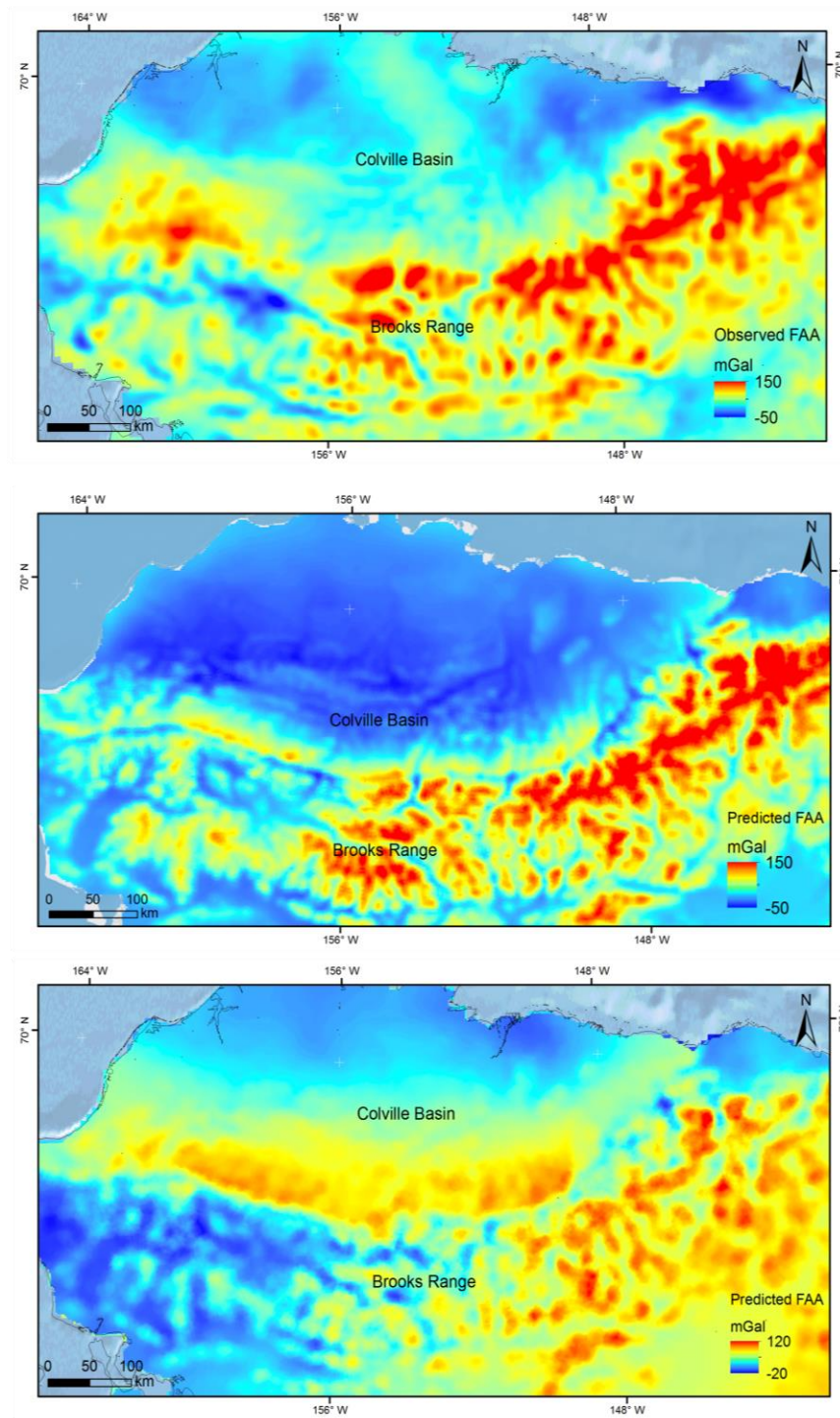
448 Accounting for sediment density variations as one of the subsurface load sources is critical for
449 calculating the right amount of applied force on the lithosphere, especially in low topographic
450 regions (e.g., see Kaban et al. 2018; Kirby & Swain, 2011; Pirouz et al., 2017). Thick Colville
451 sedimentary cover has a significant effect on the deflection, which we incorporated this vertical
452 variation into the flexural model using the borehole data; for details, see supplementary material
453 (Figure S1). Based on our flexure model, the static load associated with the Brooks Range,
454 sediment infill of Colville basin, and the subsurface load of crustal root very well define the flexure

455 of the lithosphere underneath the Arctic Alaska microplate. An additional subsurface dynamic load
456 like mantle pull is not required in the northern Alaska region to support the bending forces.

457 In contrast, Nunn et al. (1987) show that a subsurface load is needed to bend the lithosphere to
458 create desirable deflection in the Colville basin. There are several reasons for disagreement; they
459 used a simple 2D modeling approach and assumed that the geometry of the Colville basin is
460 relatively uniform. However, a detailed analysis of geometry reveals that the basin depth varies
461 abruptly adjacent to the Brooks Range (see Figure 1). Since the basin geometry is non-uniform, a
462 more robust 3D modeling technique that accounts for geometrical variations in the basin was
463 needed to accurately model the basin flexure. Next, their flexure results estimate high elastic
464 thickness values, which assume a deficit of the load compensated by replacing crustal material
465 with the mantle. The elastic strength of the lithosphere dissipates at the crust-mantle boundary,
466 with exceptions to the cratonic regions (Maggi et al., 2000). Although this view is debated from
467 the rheological viewpoint, it is considered a valid explanation for various tectonic settings, for
468 example, a rifted passive margin undergoing subsequent thrusting (Watts & Burov, 2003). Since
469 Arctic Alaska microplate also underwent thrusting subsequent with rifting, it suggests that the
470 elastic strength would most likely be associated with the crust, with little/no influence from the
471 mantle in this region. Nunn et al. (1987) used the top of the Lower Cretaceous Pebble Shale to
472 reconstruct the geometry basin, whereas we used LCU unconformity as the foreland basin depth
473 indicator. We show that the wavelength of the Colville basin is very well correlated with the size
474 of the Brooks Range along with associated crustal root that is proportional to the size of the orogen.
475 It is not suitable to invoke an additional subsurface force that would cause the deflection of the
476 Colville basin.

477 **4.4. Gravity and Flexural Support**

478 Orogenic wedge and adjacent foreland basin show positive and negative values of free air anomaly
479 in response to the flexed lithosphere during a mountain building process (Karner & Watts, 1983;
480 L. Royden & Karner, 1984). Obtained free air anomaly from geological and geophysical models
481 can be compared to the observed anomaly to evaluate the modeling results. We examined fidelity
482 of the flexural model of Arctic Alaska from modeled gravity and free air anomalies. To this
483 purpose, we calculate FAA in Arctic Alaska using two different data sources. One is based on the
484 seismic Moho depth provided by Torne et al., 2020, and the other from our flexural model (Figures
485 8 and 9). The estimated FAA from the flexural model shows that the Brooks Range is characterized
486 by 150 mGal positive value representing a thick crust, and the adjacent Colville basin shows a
487 decrease in anomalies close to -50 mGal (Figures 7 and 8). Correlation between the observed and
488 predicted FAA shows that our FAA model significantly well characterizes the Colville basin and
489 the Brooks Range signals. The northern portion of the cross-sections that spans over 200 km shows
490 a perfect fit to the observed FAA, and the southern portion shows a relatively good correlation
491 along the Brooks Range thrust belt. Calculations of FAA derived from seismic Moho (see figures
492 7 and 8) has a good overall correlation with the observed anomalies. There is a significant
493 mismatch over the basin, about 40 mGal, in which the higher values are probably due to the ignored
494 mass deficit. Modeled FAA signal in Arctic Alaska supports and validates our flexural model of
495 the Colville foreland basin. The FAA calculated by the flexural deflection model is very well
496 correlated with observed FAA anomalies with a maximum misfit of only 27 mGal. Since the FAA
497 anomalies derived from the deflection model fit well to the observed data, 13-16 km of estimated
498 effective elastic thickness is an accurate representation of elastic strength of the Arctic Alaska
499 lithosphere.



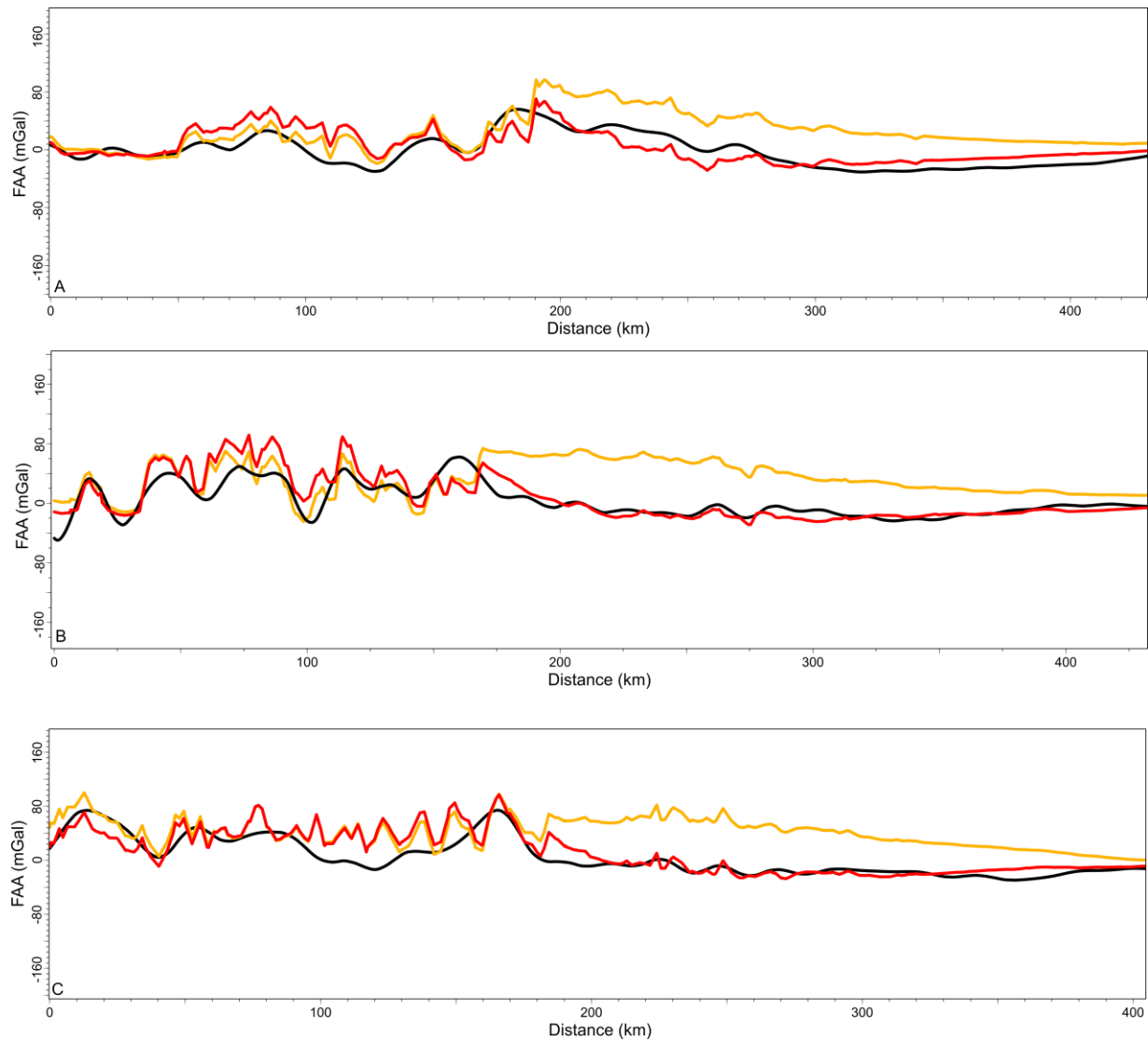
500

501 Figure 8. (a) observed, (b) predicted from the flexural model, and (c) predicted from Moho FAA. The Brooks Range is characterized by significantly

502 closer to zero anomalies (yellow) in the central thrust belt except for high values (red) where the belt extends further into the present-day shelf.

503 Colville basin has a typical foreland basin low anomaly response (blue color).

504



505

506 Figure 9. A comparison between observed FAA (black Curve; Bonvalot et al., 2012) with calculated FAA from seismic Moho (orange) (Torne et
 507 al., 2020) and deflection model (red, this study) along the sections A, B, and C. Location of sections are shown in Figure 1.

508

509

510 **4.5. Seismogenic Layer in the Brooks Range**

511 Earthquakes mostly occur in the uppermost part of the brittle and competent layer of the crustal
 512 lithosphere, supporting the elastic stresses. The seismogenic layer is usually about < 20 km, except

513 the subduction zones where deep earthquakes (~40 km) can also occur. The strength of a
514 continental lithosphere is likely contained within the seismogenic layer (Maggi et al.,
515 2000). Earthquakes may extend into deeper depth, into the brittle zone of the sub-crustal mantle
516 on major faults, in regions of high curvature or high bending stresses (Watts & Burov, 2003). In
517 southern Alaska, near the Pacific subduction zone, the reported seismogenic layer thickness is 25
518 km (Walton et al., 2019). On the other hand, until recently, mapping and characterization of active
519 faults in the northern Alaska region have been limited, mostly due to lack of geological mapping
520 and harsh climate conditions (Gaudreau et al., 2019; Gibbons et al., 2020).

521 In northern Alaska, earthquake monitoring began as early as the 1970s (Estabrook et al., 1988),
522 with moderate-sized earthquakes detected every few years. Interestingly, the recent deployment of
523 seismic networks, notably, Earthscope USArray (Ruppert & West, 2020), has shown an increase
524 in recorded earthquake activity, particularly in the northeastern Brooks Range. This increase in
525 seismicity has redrawn interest in seismological studies in northern Alaska (Gaudreau et al., 2019;
526 Gibbons et al., 2020; Xu et al., 2020). In our study area, the observed seismicity is summarized in
527 Figures 10 and 11, which shows the distribution, magnitude, and frequency histogram of a total of
528 752 seismic events (1960 to present) with a large magnitude (≥ 4 to ≤ 6.3). In northern Alaska,
529 the maximum number of earthquake frequency dissipates at depths between 10 and 15 km.
530 Seismological studies in this region indicate that the driving forces of tectonic activity mainly
531 result from deformation associated with far-field stresses originating from mantle flow and the
532 northward movement of tectonic Yakutat block due to subduction of Pacific plate at the southern
533 Alaskan margin. (Berg et al., 2020; Mazzotti et al., 2013; Mazzotti & Hyndman, 2002). These
534 evidences indicate presence of a strong mantle that serves as a guiding block in the northern Alaska

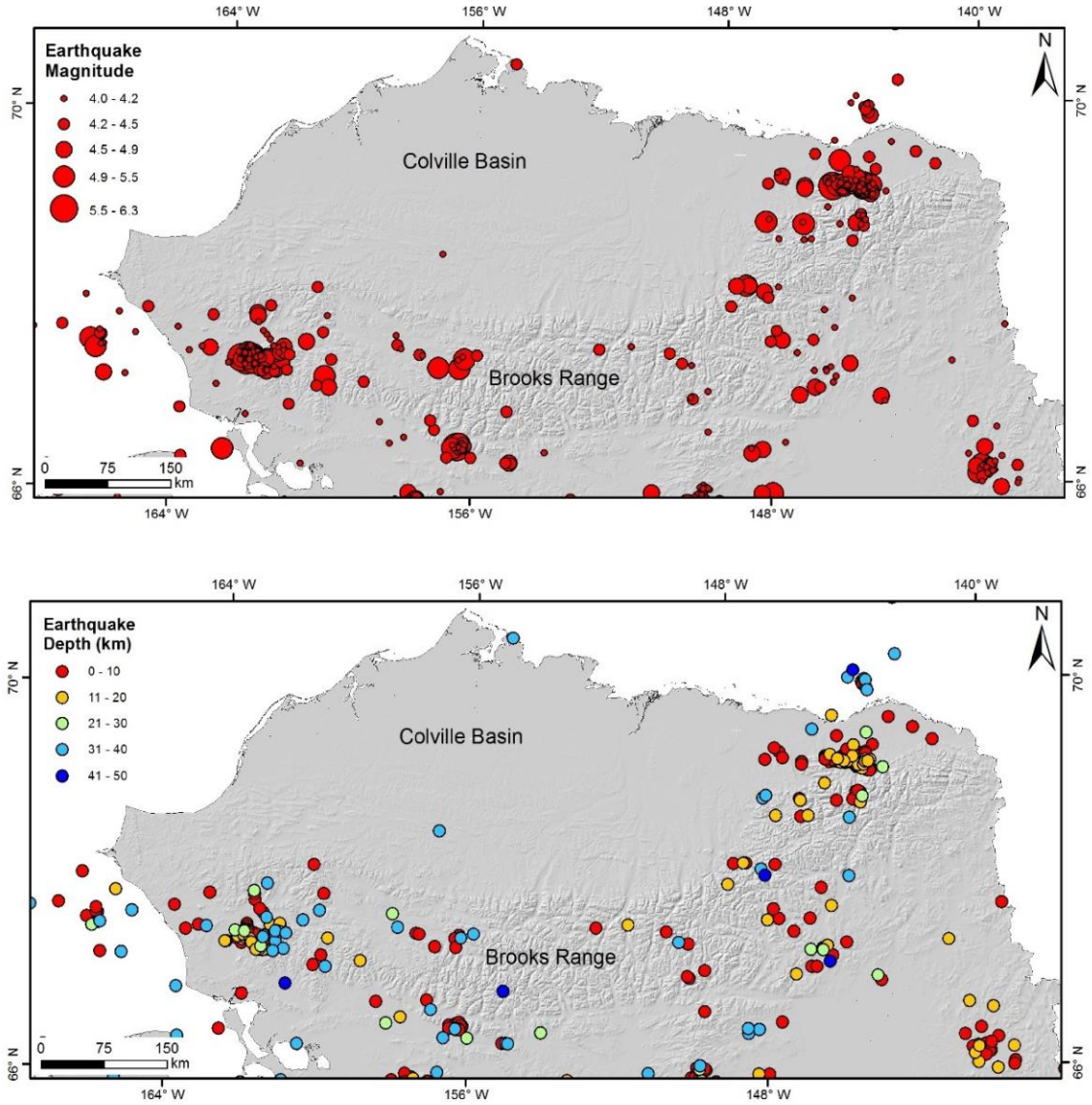
535 region for the strain transmission from the south toward north. Consequently, most of these studies
536 conclude the presence of a strong and cold lithosphere.

537 On the scale of entire Alaska and Canada, mechanically weak zones in the lithosphere and high
538 heat flow is also indicated (Mazzotti & Hyndman, 2002). Furthermore, the flexural model of this
539 study indicates weakness in the northern part of the Alaska lithosphere. To explain these
540 contrasting rheological observations, we again resort to the decoupling phenomena. We assert that
541 brittle crust and mantle decoupling is the only plausible explanation of the weak elastic lithosphere
542 with strong mantle rheology. This view is also supported by the observation of earthquakes limited
543 to the brittle part of the crust in the northern Alaska region. It implies that the elasticity diminishes
544 below this depth in the crust, which validates our computed 13-16 km elastic thickness from the
545 flexure model. For a lithospheric plate whose strength comes from subsurface mantle forces as
546 predicted previously (Nunn et al., 1987), we would expect the frequent occurrence of deep
547 earthquakes in Arctic Alaska. However, there are few sporadically recorded earthquakes in this
548 region at a depth greater than 60 km. The second peak of observed earthquakes at 40-45 km is
549 more likely correlated to the Moho boundary. Our results show that induced stresses from southern
550 Alaska have less/no influence on the lithosphere's mechanical strength in northern Alaska and the
551 Colville basin. These tectonic stresses might be localized within the substantial portion of the
552 mantle and thus only provide means of strain transfer to direct an overall northward plate motion.

553

554

555



556

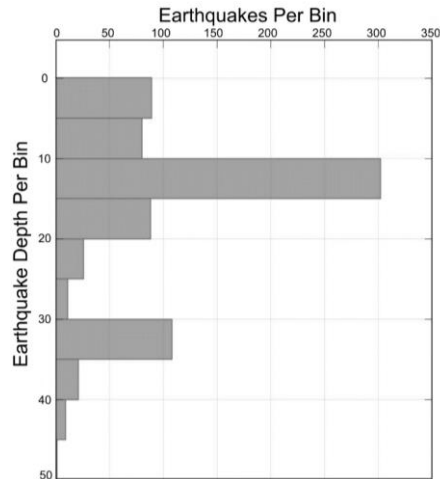
557 Figure 10. The upper panel shows locations of earthquakes with their corresponding depth. The lower panel shows the corresponding magnitude

558 of earthquakes in the Brooks Range area. Data collected from IRIS Catalog using Zmap software

559

560

561



562

563 Figure 11. Frequency distribution chart showing the maximum depth of most frequent earthquakes in the Brooks Range and Colville basin dissipates
 564 at 20 km depth.

565

566 **5. Conclusions**

567 The elastic thickness of the lithosphere is an essential feature of plate geomechanics. Our simple
 568 3D flexural modeling results quantitatively evaluate the elastic properties of the lithosphere in the
 569 northern Alaska region. The flexural model of the Colville basin with 13-16 km thickness and a
 570 load of crustal root with a scaling factor of 3.4-4.5 times of the topography provides a best-fitting
 571 model to present-day geometry of the Colville basin with 3% of average misfit error over the basin.
 572 Frequent earthquakes dissipate near 20 km depth, where the crust behaves aseismic and does not
 573 transmit significant stresses below this depth. Since the Brooks Range and the Colville basin
 574 sediment loads provide an accurate deflection of the Colville basin, there is no need to invoke an
 575 additional subsurface dynamic load as inferred previously. A comparison free air anomaly between
 576 observed, obtained from the flexural model, and derived from the Moho boundary shows an
 577 excellent correlation for the wedge and the basin area. The maximum error is only 27 mGal.

578 **Acknowledgments**

579 The authors thank Dr. Hejun Zhu and Dr. Robert Stern for their constructive feedback.

580 **Data Availability Statement**

581 No new data has been utilized in this research. The data for flexural model is available through
 582 (Bird & Houseknecht, 2011). Moho boundary dataset is available in (Torne et al., 2020). Free-air
 583 surface gravity anomalies dataset is available from (Bonvalot et al., 2012). The code to model the
 584 flexure is available from (Pirouz et al., 2017).

585 **References**

- 586 Afonso, J. C., & Ranalli, G. (2004). Crustal and mantle strengths in continental lithosphere: Is the jelly sandwich model
 587 obsolete? *Tectonophysics*, 394(3), 221–232. <https://doi.org/10.1016/j.tecto.2004.08.006>
- 588 Angrand, P., Ford, M., & Watts, A. B. (2018). Lateral Variations in Foreland Flexure of a Rifted Continental Margin: The
 589 Aquitaine Basin (SW France). *Tectonics*, 37(2), 430–449. <https://doi.org/10.1002/2017TC004670>
- 590 Arnaiz-Rodríguez, M. S., Álvarez Hostos, J. C., & Audemard, F. (2020). LIFFE: Lithospheric flexure with finite elements.
 591 *Computers & Geosciences*, 140, 104483. <https://doi.org/10.1016/j.cageo.2020.104483>
- 592 Beaumont, C. (1981). Foreland basins. *Geophysical Journal International*, 65(2), 291–329. [https://doi.org/10.1111/j.1365-
 593 246X.1981.tb02715.x](https://doi.org/10.1111/j.1365-246X.1981.tb02715.x)
- 594 Bechtel, T. D., Forsyth, D. W., Sharpton, V. L., & Grieve, R. A. F. (1990). Variations in effective elastic thickness of the
 595 North American lithosphere. *Nature*, 343(6259), 636–638. <https://doi.org/10.1038/343636a0>
- 596 Berg, E. M., Lin, F.-C., Allam, A., Schulte-Pelkum, V., Ward, K. M., & Shen, W. (2020). Shear Velocity Model of Alaska
 597 Via Joint Inversion of Rayleigh Wave Ellipticity, Phase Velocities, and Receiver Functions Across the Alaska
 598 Transportable Array. *Journal of Geophysical Research: Solid Earth*, 125(2), e2019JB018582.
 599 <https://doi.org/10.1029/2019JB018582>
- 600 Bird, K. J. (2001). Framework Geology, Petroleum Systems, and Play Concepts of the National Petroleum Reserve –
 601 Alaska. <https://doi.org/10.2110/cor.01.01.0005>
- 602 Bird, K. J., & Houseknecht, D. W. (2011). Chapter 32 Geology and petroleum potential of the Arctic Alaska petroleum
 603 province. Geological Society, London, *Memoirs*, 35(1), 485–499. <https://doi.org/10.1144/M35.32>
- 604 Bird, K. J., & Molenaar, C. M. (1992). The North Slope Foreland Basin, Alaska: Chapter 13. 136, 363–393.

- 60Bonvalot, S., Balmino, G., Briais, A., Kuhn, M., Peyrefitte, A., Vales, N., Biancale, R., Gabalda, G., & Reinquin, F.
606 (2012). World Gravity Map: A set of global complete spherical Bouguer and isostatic anomaly maps and grids. 14,
607 11091.
- 60Box, S. E. (1985). Early Cretaceous Orogenic Belt in Northwestern Alaska: Internal Organization, Lateral Extent, and
609 Tectonic Interpretation. http://archives.datapages.com/data/circ_pac/1/137_b.htm
- 61Braitenberg, C., Ebbing, J., & Goetze, H. (2002). Inverse modelling of elastic thickness by convolution method – the
611 eastern Alps as a case example. [https://doi.org/10.1016/S0012-821X\(02\)00793-8](https://doi.org/10.1016/S0012-821X(02)00793-8)
- 61Brown, C. D., & Phillips, R. J. (2000). Crust-mantle decoupling by flexure of continental lithosphere. *Journal of*
613 *Geophysical Research: Solid Earth*, 105(B6), 13221–13237. <https://doi.org/10.1029/2000JB900069>
- 61Burov, E B. (2006). The long-term strength of continental lithosphere: “Jelly sandwich” or “crème brûlée”? *GSA*
615 *TODAY*, 7.
- 61Burov, Evgene B., & Diament, M. (1995). The effective elastic thickness (T_e) of continental lithosphere: What does it
617 really mean? *Journal of Geophysical Research: Solid Earth*, 100(B3), 3905–3927.
618 <https://doi.org/10.1029/94JB02770>
- 61Cattin, R., Martelet, G., Henry, P., Avouac, J. P., Diament, M., & Shakya, T. R. (2001). Gravity anomalies, crustal
620 structure and thermo-mechanical support of the Himalaya of Central Nepal. *Geophysical Journal International*,
621 147(2), 381–392. <https://doi.org/10.1046/j.0956-540x.2001.01541.x>
- 62Cole, F., Bird, K. J., Toro, J., Roure, F., O’Sullivan, P. B., Pawlewicz, M., & Howells, D. G. (1997). An integrated model
623 for the tectonic development of the frontal Brooks Range and Colville Basin 250 km west of the Trans-Alaska
624 Crustal Transect. *Journal of Geophysical Research: Solid Earth*, 102(B9), 20685–20708.
625 <https://doi.org/10.1029/96JB03670>
- 62Curry, M. E., van der Beek, P., Huisman, R. S., Wolf, S. G., & Muñoz, J.-A. (2019). Evolving paleotopography and
627 lithospheric flexure of the Pyrenean Orogen from 3D flexural modeling and basin analysis. *Earth and Planetary*
628 *Science Letters*, 515, 26–37. <https://doi.org/10.1016/j.epsl.2019.03.009>
- 62DeCelles, P. G. (2012). Foreland Basin Systems Revisited: Variations in Response to Tectonic Settings. In *Tectonics of*
630 *Sedimentary Basins* (pp. 405–426). John Wiley & Sons, Ltd. <https://doi.org/10.1002/9781444347166.ch20>
- 63Decker, P. L. (2007). Brookian sequence stratigraphic correlations, Umiat Field to Milne Point Field, west-central North
632 Slope, Alaska (PIR 2007-2; p. PIR 2007-2). Alaska Division of Geological & Geophysical Surveys.
633 <https://doi.org/10.14509/15758>
- 63Desegaulx, P., Kooi, H., & Cloetingh, S. (1991). Consequences of foreland basin development on thinned continental
635 lithosphere: Application to the Aquitaine basin (SW France). *Earth and Planetary Science Letters*, 106(1), 116–132.
636 [https://doi.org/10.1016/0012-821X\(91\)90067-R](https://doi.org/10.1016/0012-821X(91)90067-R)

- 63Embry, A. F. (1990). Geological and geophysical evidence in support of the hypothesis of anticlockwise rotation of
638 northern Alaska. *Marine Geology*, 93, 317–329. [https://doi.org/10.1016/0025-3227\(90\)90090-7](https://doi.org/10.1016/0025-3227(90)90090-7)
- 63Eshagh, M., Tenzer, R., & Eshagh, M. (2020). Elastic thickness of the Iranian lithosphere from gravity and seismic data.
640 *Tectonophysics*, 774, 228186. <https://doi.org/10.1016/j.tecto.2019.228186>
- 64Estabrook, C. H., Stone, D. B., & Davies, J. N. (1988). Seismotectonics of northern Alaska. *Journal of Geophysical*
642 *Research: Solid Earth*, 93(B10), 12026–12040. <https://doi.org/10.1029/JB093iB10p12026>
- 64Forsyth, D. W. (1985). Subsurface loading and estimates of the flexural rigidity of continental lithosphere. *Journal of*
644 *Geophysical Research: Solid Earth*, 90(B14), 12623–12632. <https://doi.org/10.1029/JB090iB14p12623>
- 64Fosdick, J. C., Graham, S. A., & Hilley, G. E. (2014). Influence of attenuated lithosphere and sediment loading on flexure
646 of the deep-water Magallanes retroarc foreland basin, Southern Andes. *Tectonics*, 33(12), 2505–2525.
647 <https://doi.org/10.1002/2014TC003684>
- 64Fuis, Gary S., Moore, T. E., Plafker, G., Brocher, T. M., Fisher, M. A., Mooney, W. D., Nokleberg, W. J., Page, R. A.,
649 Beaudoin, B. C., Christensen, N. I., Levander, A. R., Lutter, W. J., Saltus, R. W., & Ruppert, N. A. (2008). Trans-
650 Alaska Crustal Transect and continental evolution involving subduction underplating and synchronous foreland
651 thrusting. *Geology*, 36(3), 267–270. <https://doi.org/10.1130/G24257A.1>
- 65Fuis, G.S., Murphy, J. M., Lutter, W. J., Moore, T. E., Bird, K. J., & Christensen, N. I. (1997). Deep seismic structure and
653 tectonics of northern Alaska: Crustal-scale duplexing with deformation extending into the upper mantle. *Journal of*
654 *Geophysical Research B: Solid Earth*, 102(B9), 24.
- 65Garcia-Castellanos, D. (2002). Interplay between lithospheric flexure and river transport in foreland basins. *Basin*
656 *Research*, 14(2), 89–104. <https://doi.org/10.1046/j.1365-2117.2002.00174.x>
- 65Garcia-Castellanos, D., Fernández, M., & Torne, M. (1997). Numerical modeling of foreland basin formation: A program
658 relating thrusting, flexure, sediment geometry and lithosphere rheology. *Computers & Geosciences*, 23(9), 993–
659 1003. [https://doi.org/10.1016/S0098-3004\(97\)00057-5](https://doi.org/10.1016/S0098-3004(97)00057-5)
- 66Caudreau, É., Nissen, E. K., Bergman, E. A., Benz, H. M., Tan, F., & Karasözen, E. (2019). The August 2018 Kaktovik
661 Earthquakes: Active Tectonics in Northeastern Alaska Revealed With InSAR and Seismology. *Geophysical*
662 *Research Letters*, 46(24), 14412–14420. <https://doi.org/10.1029/2019GL085651>
- 66Gibbons, S. J., Ruppert, N. A., Karasözen, E., Aderhold, K., & Dickson, I. (2020). Resolving Northern Alaska Earthquake
664 Sequences Using the Transportable Array and Probabilistic Location Methods. *Seismological Research Letters*.
665 <https://doi.org/10.1785/0220200142>
- 66Grantz, A., & May, S. D. (1982). Rifting history and structural development of the continental margin north of Alaska. In
667 *American Association of Petroleum Geologists (Ed.), M 34: Studies in continental margin geology (pp. 77–100).*

- 668 American Association of Petroleum Geologists; USGS Publications Warehouse.
669 <http://pubs.er.usgs.gov/publication/70186628>
- 670 Grantz, A., May, S. D., & Hart, P. E. (1994). Geology of the Arctic continental margin of Alaska. In G. Plafker & H. C.
671 Berg (Eds.), *The Geology of Alaska* (pp. 17–48). Geological Society of America. [https://doi.org/10.1130/DNAG-](https://doi.org/10.1130/DNAG-GNA-G1.17)
672 [GNA-G1.17](https://doi.org/10.1130/DNAG-GNA-G1.17)
- 673 Haddad, D., & Watts, A. B. (1999). Subsidence history, gravity anomalies, and flexure of the northeast Australian margin
674 in Papua New Guinea. *Tectonics*, 18(5), 827–842. <https://doi.org/10.1029/1999TC900009>
- 675 Houseknecht, D. W. (2019). Chapter 18—Evolution of the Arctic Alaska Sedimentary Basin. In A. D. Miall (Ed.), *The*
676 *Sedimentary Basins of the United States and Canada (Second Edition)* (pp. 719–745). Elsevier.
677 <https://doi.org/10.1016/B978-0-444-63895-3.00018-8>
- 678 Houseknecht, D. W., Bird, K. J., & Schenk, C. J. (2009). Seismic analysis of clinoform depositional sequences and shelf-
679 margin trajectories in Lower Cretaceous (Albian) strata, Alaska North Slope. *Basin Research*, 21(5), 644–654.
680 <https://doi.org/10.1111/j.1365-2117.2008.00392.x>
- 681 Houseknecht, D. W., & Wartes, M. A. (2013). Clinoform deposition across a boundary between orogenic front and
682 foredeep—An example from the Lower Cretaceous in Arctic Alaska. *Terra Nova*, 25(3), 206–211.
683 <https://doi.org/10.1111/ter.12024>
- 684 Hubbard, R. J., Edrich, S. P., & Peter Rattey, R. (1987). Geologic evolution and hydrocarbon habitat of the ‘Arctic Alaska
685 Microplate.’ *Marine and Petroleum Geology*, 4(1), 2–34. [https://doi.org/10.1016/0264-8172\(87\)90019-5](https://doi.org/10.1016/0264-8172(87)90019-5)
- 686 Jackson, J. (2002). Strength of the continental lithosphere: Time to abandon the jelly sandwich? *GSA TODAY*, 6.
- 687 Kaban, M. K., Chen, B., Tesauero, M., Petrunin, A. G., Khrepy, S. E., & Al-Arifi, N. (2018). Reconsidering Effective
688 Elastic Thickness Estimates by Incorporating the Effect of Sediments: A Case Study for Europe. *Geophysical*
689 *Research Letters*, 45(18), 9523–9532. <https://doi.org/10.1029/2018GL079732>
- 690 Karner, G. D., & Watts, A. B. (1983). Gravity anomalies and flexure of the lithosphere at mountain ranges. *Journal of*
691 *Geophysical Research: Solid Earth*, 88(B12), 10449–10477. <https://doi.org/10.1029/JB088iB12p10449>
- 692 Kirby, J. F., & Swain, C. J. (2009). A reassessment of spectral Te estimation in continental interiors: The case of North
693 America. *Journal of Geophysical Research: Solid Earth*, 114(B8). <https://doi.org/10.1029/2009JB006356>
- 694 Kirby, J. F., & Swain, C. J. (2011). Improving the spatial resolution of effective elastic thickness estimation with the fan
695 wavelet transform. *Computers & Geosciences*, 37(9), 1345–1354. <https://doi.org/10.1016/j.cageo.2010.10.008>
- 696 Yin, A. T., & Watts, A. B. (2002). Origin of the West Taiwan basin by orogenic loading and flexure of a rifted continental
697 margin. *Journal of Geophysical Research: Solid Earth*, 107(B9), ETG 2-1-ETG 2-19.
698 <https://doi.org/10.1029/2001JB000669>

- 69Dyon-Caen, H., & Molnar, P. (1983). Constraints on the structure of the Himalaya from an analysis of gravity anomalies
700 and a flexural model of the lithosphere. *Journal of Geophysical Research: Solid Earth*, 88(B10), 8171–8191.
701 <https://doi.org/10.1029/JB088iB10p08171>
- 70Maggi, A., Jackson, J. A., McKenzie, D., & Priestley, K. (2000). Earthquake focal depths, effective elastic thickness, and
703 the strength of the continental lithosphere. *Geology*, 28(6), 495–498. [https://doi.org/10.1130/0091-7613\(2000\)28<495:EFDEET>2.0.CO;2](https://doi.org/10.1130/0091-7613(2000)28<495:EFDEET>2.0.CO;2)
- 70Mayfield, C. F., Tailleur, I. L., & Ellersieck, I. (1983). Stratigraphy, structure, and palinspastic synthesis of the western
706 Brooks Range, northwestern Alaska (USGS Numbered Series No. 83–779; Open-File Report). U.S. Geological
707 Survey,. <http://pubs.er.usgs.gov/publication/ofr83779>
- 70Mazzotti, Stéphane, & Hyndman, R. D. (2002). Yakutat collision and strain transfer across the northern Canadian
709 Cordillera. *Geology*, 30(6), 495–498. [https://doi.org/10.1130/0091-7613\(2002\)030<0495:YCASTA>2.0.CO;2](https://doi.org/10.1130/0091-7613(2002)030<0495:YCASTA>2.0.CO;2)
- 71Mazzotti, Stephane, Leonard, L. J., Hyndman, R. D., & Cassidy, J. F. (2013). Tectonics, Dynamics, and Seismic Hazard in
711 the Canada-Alaska Cordillera. In J. T. Freymueller, P. J. Haeussler, R. L. Wesson, & G. Ekström (Eds.),
712 *Geophysical Monograph Series* (pp. 297–319). American Geophysical Union. <https://doi.org/10.1029/179GM17>
- 71McKenzie, D. (2010). The influence of dynamically supported topography on estimates of T_e . *Earth and Planetary
714 Science Letters*, 295(1), 127–138. <https://doi.org/10.1016/j.epsl.2010.03.033>
- 71McKenzie, D., & Fairhead, D. (1997). Estimates of the effective elastic thickness of the continental lithosphere from
716 Bouguer and free air gravity anomalies. *Journal of Geophysical Research: Solid Earth*, 102(B12), 27523–27552.
717 <https://doi.org/10.1029/97JB02481>
- 71Miller, M. S., O'Driscoll, L. J., Porritt, R. W., & Roeske, S. M. (2018). Multiscale crustal architecture of Alaska inferred
719 from P receiver functions. *Lithosphere*, 10(2), 267–278. <https://doi.org/10.1130/L701.1>
- 72Miller, T. P. (1994). Pre-Cenozoic plutonic rocks in mainland Alaska. In G. Plafker & H. C. Berg (Eds.), *The Geology of
721 Alaska* (pp. 535–554). Geological Society of America. <https://doi.org/10.1130/DNAG-GNA-G1.535>
- 72Moore, T. E., & Box, S. E. (2016). Age, distribution and style of deformation in Alaska north of 60°N: Implications for
723 assembly of Alaska. *Tectonophysics*, 691, 133–170. <https://doi.org/10.1016/j.tecto.2016.06.025>
- 72Moore, T. E., Potter, C. J., O'Sullivan, P. B., Shelton, K. L., & Underwood, M. B. (2004). Two stages of deformation and
725 fluid migration in the central Brooks Range fold-and-thrust belt. In *AAPG Bulletin* (Vol. 1, p. 20).
- 72Moore, T. E., Wallace, W. K., Bird, K. J., Karl, S. M., Mull, C. G., & Dillon, J. T. (1994). Geology of northern Alaska. In
727 G. Plafker & H. C. Berg (Eds.), *The Geology of Alaska* (pp. 49–140). Geological Society of America.
728 <https://doi.org/10.1130/DNAG-GNA-G1.49>
- 72Mull, C. G. (1982). Tectonic Evolution and Structural Style of the Brooks Range, Alaska: An Illustrated Summary.
730 http://archives.datapages.com/data/rmag/GeoStudCordV1_82/mull.htm

- 731 Nunn, J. A., Czerniak, M., & Pilger, R. H. (1987). Constraints on the structure of Brooks Range and Colville Basin,
732 northern Alaska, from flexure and gravity analysis. *Tectonics*, 6(5), 603–617.
733 <https://doi.org/10.1029/TC006i005p00603>
- 734 Patton, W. W., & Box, S. E. (1989). Tectonic setting of the Yukon-Koyukuk Basin and its borderlands, western Alaska.
735 *Journal of Geophysical Research: Solid Earth*, 94(B11), 15807–15820. <https://doi.org/10.1029/JB094iB11p15807>
- 736 Patton, W. W., Box, Stephen. E., & Grybeck, D. J. (1994). Ophiolites and other mafic-ultramafic complexes in Alaska. In
737 G. Plafker & H. C. Berg (Eds.), *The Geology of Alaska* (pp. 671–686). Geological Society of America.
738 <https://doi.org/10.1130/DNAG-GNA-G1.671>
- 739 Pirouz, M., Avouac, J.-P., Gualandi, A., Hassanzadeh, J., & Sternai, P. (2017). Flexural bending of the Zagros foreland
740 basin. *Geophysical Journal International*, 210(3), 1659–1680. <https://doi.org/10.1093/gji/ggx252>
- 741 Pirouz, M., Avouac, J.-P., Gualandi, A., Quddusi, M. H., & Huang, W. (2020). New Versus Conventional Approach for
742 Modeling Flexure of Foreland Basins (No. EGU2020-13016). EGU2020. Copernicus Meetings.
743 <https://doi.org/10.5194/egusphere-egu2020-13016>
- 744 Plafker, G., & Berg, H. C. (1994). Overview of the geology and tectonic evolution of Alaska. In *The Geology of Alaska*
745 (pp. 989–1021). Geological Society of America. <https://doi.org/10.1130/DNAG-GNA-G1.989>
- 746 Royden, L., & Karner, G. D. (1984). Flexure of Lithosphere Beneath Apennine and Carpathian Foredeep Basins: Evidence
747 for an Insufficient Topographic Load. *AAPG Bulletin*, 68(6), 704–712.
- 748 Ruppert, N. A., & West, M. E. (2020). The Impact of USArray on Earthquake Monitoring in Alaska. *Seismological*
749 *Research Letters*, 91(2A), 601–610. <https://doi.org/10.1785/0220190227>
- 750 Simpson, G. (2017). *Practical finite element modeling in earth science using Matlab*. John Wiley & Sons.
- 751 Stier, N. E., Connors, C. D., & Houseknecht, D. W. (2014). Influence of the Kingak Shale ultimate shelf margin on frontal
752 structures of the Brooks Range in the National Petroleum Reserve in Alaska (USGS Numbered Series No. 2014–
753 5056; Scientific Investigations Report, p. 20). U.S. Geological Survey.
754 <http://pubs.er.usgs.gov/publication/sir20145056>
- 755 Sweeney, J. F. (1985). Comments about the age of the Canada Basin. *Tectonophysics*, 114(1), 1–10.
756 [https://doi.org/10.1016/0040-1951\(85\)90004-6](https://doi.org/10.1016/0040-1951(85)90004-6)
- 757 Tesauro, M., Audet, P., Kaban, M. K., Bürgmann, R., & Cloetingh, S. (2012). The effective elastic thickness of the
758 continental lithosphere: Comparison between rheological and inverse approaches. *Geochemistry, Geophysics,*
759 *Geosystems*, 13(9). <https://doi.org/10.1029/2012GC004162>
- 760 Will, A. B. (2016). A synthesis of Jurassic and Early Cretaceous crustal evolution along the southern margin of the Arctic
761 Alaska–Chukotka microplate and implications for defining tectonic boundaries active during opening of Arctic
762 Ocean basins. *Lithosphere*, 8(3), 219–237. <https://doi.org/10.1130/L471.1>

- 76Torne, M., Jiménez–Munt, I., Vergés, J., Fernández, M., Carballo, A., & Jadamec, M. (2020). Regional crustal and
 764 lithospheric thickness model for Alaska, the Chukchi shelf, and the inner and outer Bering shelves. *Geophysical*
 765 *Journal International*, 220(1), 522–540. <https://doi.org/10.1093/gji/ggz424>
- 766Curcotte, D. L., & Schubert, G. (2002). *Geodynamics—2nd Edition*. <https://doi.org/10.2277/0521661862>
- 76Wallace, W. K., Moore, T. E., & Plafker, G. (1997). Multistory duplexes with forward dipping roofs, north central Brooks
 768 Range, Alaska. *Journal of Geophysical Research: Solid Earth*, 102(B9), 20773–20796.
 769 <https://doi.org/10.1029/96JB02682>
- 77Walton, M. A. L., Roland, E. C., Walter, J. I., Gulick, S. P. S., & Dotray, P. J. (2019). Seismic velocity structure across the
 771 2013 Craig, Alaska rupture from aftershock tomography: Implications for seismogenic conditions. *Earth and*
 772 *Planetary Science Letters*, 507, 94–104. <https://doi.org/10.1016/j.epsl.2018.11.021>
- 77Watts, A. B. (1992). The effective elastic thickness of the lithosphere and the evolution of foreland basins. *Basin*
 774 *Research*, 4(3–4), 169–178. <https://doi.org/10.1111/j.1365-2117.1992.tb00043.x>
- 77Watts, A. B. (2001). *Isostasy and flexure of the lithosphere*. Cambridge University Press.
- 77Watts, A. B., & Burov, E. B. (2003). Lithospheric strength and its relationship to the elastic and seismogenic layer
 777 thickness. *Earth and Planetary Science Letters*, 213(1), 113–131. [https://doi.org/10.1016/S0012-821X\(03\)00289-9](https://doi.org/10.1016/S0012-821X(03)00289-9)
- 77Wiemer, S. (2001). A Software Package to Analyze Seismicity: ZMAP. *Seismological Research Letters*, 72(3), 373–382.
 779 <https://doi.org/10.1785/gssrl.72.3.373>
- 78Wienecke, S., Braitenberg, C., & Götze, H.-J. (2007). A new analytical solution estimating the flexural rigidity in the
 781 Central Andes. *Geophysical Journal International*, 169(3), 789–794. [https://doi.org/10.1111/j.1365-](https://doi.org/10.1111/j.1365-246X.2007.03396.x)
 782 [246X.2007.03396.x](https://doi.org/10.1111/j.1365-246X.2007.03396.x)
- 78Xu, G., Xu, C., Wen, Y., Xiong, W., & Valkaniotis, S. (2020). The Complexity of the 2018 Kaktovik Earthquake
 784 Sequence in the Northeast of the Brooks Range, Alaska. *Geophysical Research Letters*, 47(19), e2020GL088012.
 785 <https://doi.org/10.1029/2020GL088012>
- 786
- 787